PHYSICAL REVIEW B **96**, 121111(R) (2017)

Ultrahigh magnetic field spectroscopy reveals the band structure of the three-dimensional topological insulator Bi_2Se_3

A. Miyata,[1] Z. Yang,[1] A. Surrente,[1] O. Drachenko,[1] D. K. Maude,[1] O. Portugall,[1]
L. B. Duffy,[2] T. Hesjedal,[2] P. Plochocka,[1] and R. J. Nicholas[2,*]
[1]*Laboratoire National des Champs Magnetiques Intenses, CNRS-UGA-UPS-INSA, 143 Avenue de Rangueil, 31400 Toulouse, France*
[2]*Clarendon Laboratory, University of Oxford, Parks Road, Oxford OX1 3PU, United Kingdom*
(Received 31 May 2017; published 18 September 2017)

We have investigated the band structure at the Γ point of the three-dimensional topological insulator Bi_2Se_3 using magnetospectroscopy over a wide range of energies (0.55–2.2 eV) and in ultrahigh magnetic fields up to 150 T. At high energies ($E > 0.6$ eV) the parabolic approximation for the massive Dirac fermions breaks down and the Landau-level dispersion becomes nonlinear. At higher energies around 0.99 and 1.6 eV, additional strong absorptions are observed with temperature and magnetic field dependences which suggest that they originate from higher band gaps. Spin-orbit splittings for the further lying conduction and valence bands are found to be 0.196 and 0.264 eV.

DOI: 10.1103/PhysRevB.96.121111

Topological insulators, which have a finite insulating band gap in the bulk form, but which can become gapless at the surface, have been intensively investigated as a new class of quantum matter [1–3]. Their surface states have topologically protected Dirac fermions with spins locked to their translational momentum due to a strong spin-orbit coupling, giving them considerable potential to be used in future electronic and spintronic devices [4,5]. The experimental observation of a single Dirac cone in the surface state by angle-resolved photoemission spectroscopy (ARPES) was reported for Bi_2Se_3 [6,7], Bi_2Te_3 [8], and Sb_2Te_3 [9], confirming that they are three-dimensional (3D) topological insulators with large band gaps in the bulk (0.1–0.3 eV). This observation stimulated a large body of work to investigate the unconventional properties arising from the topological surface states. However, there have been few experimental studies of their band structures in the bulk, despite the fact that the origin of topological surface states is critically dependent on the band inversion in the bulk crystal. In Bi_2Se_3, the bulk band structure has been described using a massive Dirac Hamiltonian with a negative mass parameter caused by band inversion due to strong spin-orbit coupling [10,11]. While ARPES studies have reported the existence of a camelbacklike band structure at the Γ point "near the surface" of Bi_2Se_3 consistent with the band inversion in the bulk [7], other techniques such as magnetotransport and infrared spectroscopy favor a bulk behavior with a direct band gap at the Γ point (i.e., no camelbacklike structure) [12,13]. The latter results are supported by theoretical GW calculations [14,15] which suggest that electron-electron interactions suppress the camelbacklike structure in the bulk bands of Bi_2Se_3.

Magneto-optical studies recently revealed the band character in the bulk of Bi_2Se_3, which has been described by a massive Dirac Hamiltonian with a negative mass term [16]. Remarkably, the observed evolution of the Landau-level energies in Bi_2Se_3 remain linear even up to 32 T, indicating that for the energies investigated ($E < 0.6$ eV), the band dispersion in the bulk of Bi_2Se_3 is almost perfectly parabolic. The GW calculations [14,15] have suggested the existence of higher direct band gaps at the Γ point, in the near infrared and visible range. The higher conduction and valence band can influence carriers in the lower bands, especially in the presence of an applied magnetic field. To date, only limited evidence of the higher band transitions has been presented [17] from fitting of the dielectric function at room temperature.

In this Rapid Communication, we present magneto-optical studies of single-crystal thin-film (110 nm) n-type Bi_2Se_3 using ultrahigh magnetic fields up to 150 T over a wide range of energies (0.55–2.2 eV). The single-crystal thin films are grown on c-plane sapphire substrates using molecular beam epitaxy, as described in detail in Refs. [18,19]. We reveal the nonlinear magnetic field evolution of the Landau levels of fundamental bands in the bulk form of Bi_2Se_3, which is explained by the massive Dirac model with the negative mass term. At high energies, ∼0.99 and 1.6 eV, additional strong absorptions are observed. From their temperature and magnetic field dependence, they are assigned as the lowest interband Landau-level transitions of the second and third band gaps, respectively.

Figure 1(a) shows representative differential (normalized by dividing by zero-field spectra) transmission spectra $T(B)/T(0)$ in Bi_2Se_3 taken at 35, 47, 60, and 67 T, which reveal a number of well-resolved absorption minima. At energies below 0.95 eV, we observe features due to inter-Landau-level absorption across the direct gap (transitions labeled E_1) at the Γ point. To study these absorptions in detail, we performed magnetic-field-dependent measurements up to 150 T, using an explosive single-turn coil and single-frequency sources [20]. Figure 1(b) shows normalized magnetotransmission $T(B)/T(0)$ of Bi_2Se_3 for excitation energies of 0.775, 0.800, 0.810, and 0.886 eV around $T = 7$ K up to 150 T. The transmission minima denoted by triangular symbols in Fig. 1(b) show clear shifts to higher magnetic fields with increasing energies, which correspond to the interband Landau-level transitions of the fundamental band gap (∼0.2 eV) in the bulk of Bi_2Se_3 [16].

Figure 2(a) shows the Landau-level fan chart combining our transmission data with the low-energy data of Orlita *et al.* [16].

*r.nicholas@physics.ox.ac.uk

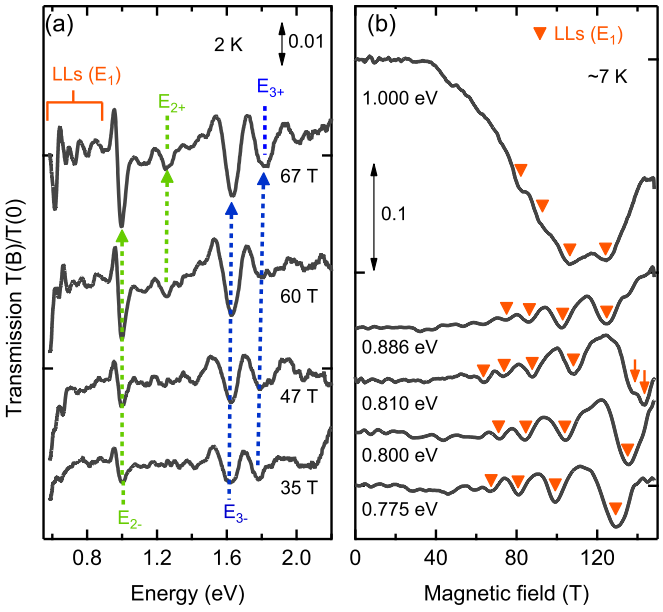

FIG. 1. (a) Low-temperature differential transmission spectra of Bi_2Se_3 at different magnetic fields of 35, 47, 60, and 67 T. (b) Magnetotransmission of Bi_2Se_3 at different energies at 7 K. (a), (b) Spectra were shifted vertically for clarity.

The dipole-allowed ($\Delta n = \pm 1$) interband inter-Landau-level transitions are fitted using the 4×4 massive Dirac Hamiltonian [10,11] which yields nonparabolic dispersion relations of the form

$$\mathcal{E}_{c,v} = Ck^2 \pm \sqrt{(\Delta + Mk^2)^2 + \hbar^2 v_D^2 k^2}, \qquad (1)$$

where 2Δ is the band gap, the interband coupling is given by v_D, known as the Dirac velocity, M is the diagonal dispersion term which is negative for materials with a band inversion, known as the negative mass term, and C is a term to account for the electron-hole asymmetry. The magnetic field solutions for this Hamiltonian [10,11] reproduce the data perfectly, with a band gap of $2\Delta = 0.19$ eV, Fermi velocity $v_D = (0.465 \pm 0.05) \times 10^6$ m/s, and a negative mass term

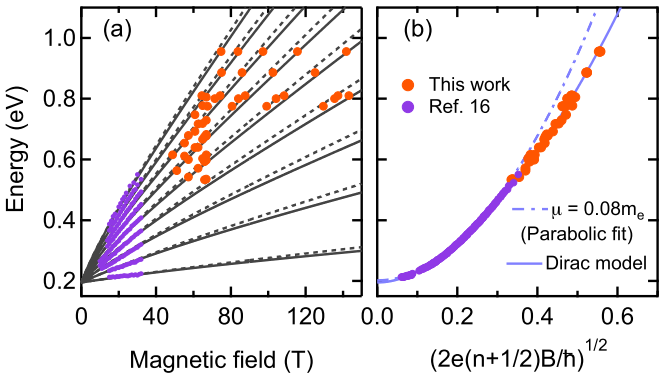

FIG. 2. (a) Low-temperature interband Landau-level fan chart for the first (fundamental) band gap in Bi_2Se_3. Dashed and solid lines are interband Landau levels obtained by the 4×4 massive Dirac Hamiltonian with electron-hole asymmetry. (b) Energy-momentum dispersion of Bi_2Se_3. The dashed line shows the fitting for parabolic dispersion.

$M = -(17 \pm 0.5)$ eV Å^2. The electron-hole asymmetry parameter $C = (3 \pm 0.5)$ eV Å^2 was determined from the observed splitting of the higher interband Landau-level transition, indicated by arrows in Fig. 1(b).

Our fitting parameters are identical within experimental error with those obtained by Orlita *et al.* [16], with the important exception of the negative mass term. Our higher-energy data place stronger constraints on the value of M and our value of $|M| = 17$ eV Å^2 is roughly 25% smaller than found by fitting to the low-energy data of Orlita *et al.* This implies that the condition $\hbar^2 v_D^2 = -4M\Delta$, required in the Dirac model to have a strictly parabolic dispersion over a wide energy range, is not fulfilled as well as previously thought. We have $\hbar^2 v_D^2 \simeq 9.6$ eV^2 Å^2 but with a significantly smaller value for $-4M\Delta \simeq 6.8$ eV^2 Å^2. This also has implications for the magnetic field $B_c = \hbar\Delta/|eM|$ at which the $n = 0$ Landau levels of the conduction and valence bands cross. The lower value of $|M|$ found here shifts B_c to a higher magnetic field ($B_c \simeq 390$ T compared to the value of around 300 T estimated by Orlita *et al.*).

In Fig. 2(b), the experimentally obtained interband Landau-level transition energies, with different indexes, are scaled into the same energy-momentum dispersion of Bi_2Se_3, deduced from the relation between the momentum k and magnetic field B. Neglecting electron-hole asymmetry, and assuming a parabolic dispersion, the energy of a dipole-allowed transition $n \to n+1$ or $n+1 \to n$ is given by $E_n = 2\Delta + [(n+\gamma+1)+(n+\gamma)]\hbar\omega_c$, with $\gamma = 0$ for massive Dirac particles. This can be rewritten using the reduced exciton mass $\mu = m^*/2$ to give $E_n = 2\Delta + (n+1/2)\hbar eB/\mu$. Equating the magnetic energy to $\hbar^2 k^2/2\mu$ gives an expression for the k vector $k = \sqrt{2eB(n+1/2)/\hbar}$, which is equivalent to the Bohr-Sommerfeld quantization of area in k space which is independent of the particle mass values assumed. In the plot of the observed transition energies versus $k = \sqrt{2eB(n+1/2)/\hbar}$, all the data collapse onto a single curve. The dashed line in Fig. 2(b) shows a parabolic dispersion using a band gap $2\Delta = 0.2$ eV and reduced exciton mass $\mu = 0.08m_0$ (m_0 is the free-electron mass). For energies above 0.6 eV a clear deviation from the simple parabolic model is observed, reflecting the transition towards a $\sqrt{B}$ dependence for the energy of Dirac fermions, which is clearly visible in Fig. 2(a). The reduced mass is consistent with recent results obtained by Shubnikov–de Haas (SdH) measurements for n- and p-type samples of Bi_2Se_3; the range of effective masses of the electrons and holes respectively is $0.12m_0$–$0.16m_0$ and $0.23m_0$–$0.25m_0$ in the literature [13,21,22], corresponding to a value for the reduced mass μ in the range $0.079m_0$–$0.098m_0$. It is also possible to estimate the effective masses from the Fermi velocity v_D and the electron-hole asymmetry term C using $m_e = 2\hbar^2/(\hbar^2 v_D^2/\Delta + 4C)$ and $m_h = 2\hbar^2/(\hbar^2 v_D^2/\Delta - 4C)$, giving $m_e = 0.138m_0$ and $m_h = 0.176m_0$, respectively.

Figure 3(a) shows the magnetotransmission of Bi_2Se_3 for temperatures from 7 to 300 K with an excitation energy of 0.810 eV. The interband Landau-level transitions of the fundamental band gap show a clear shift to higher magnetic fields with increasing temperatures. The observed shift cannot be attributed to a temperature dependence of the fundamental

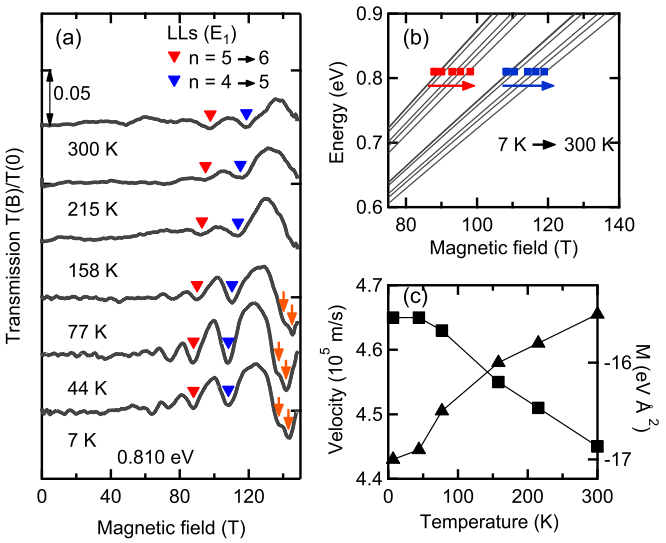

FIG. 3. (a) Magnetotransmittance of Bi_2Se_3 at the energy of 0.810 eV measured for different temperatures in fields up to 150 T. The position of the inter-Landau-level transitions are indicated by triangles. The splitting due to electron-hole asymmetry is indicated by arrows. The spectra have been shifted vertically for clarity. (b) Energy of transitions at 7 and 300 K (symbols). The solid lines are fits to the Dirac-like Hamiltonian. (c) Extracted Fermi velocity (squares) and negative mass parameter (triangles) vs temperature.

band-gap energy 2Δ in the massive Dirac model as the avoided band crossing at low energies has almost no influence on the high-energy interband Landau-level transitions. Instead, we argue that this is due to a temperature dependence of the Fermi velocity and the negative mass parameter. In Fig. 3(b) we plot the observed transition energies at 7 and 300 K together with the transition energies calculated using the Dirac-like Hamiltonian. From these we deduce, in Fig. 3(c), the temperature dependence of v_D and M. By 300 K the Fermi velocity has dropped to $v_D = 0.445 \times 10^6$ m/s, significantly ($\simeq$6%) lower than the low-temperature value, and the negative mass parameter has changed by around 10% to $M \simeq -15.5\,\text{eV}\,\text{Å}^2$ at 300 K.

We now turn our attention to the transitions observed at higher energies in Fig. 1(a). There is clear evidence for a second band gap, with a pair of absorptions at 0.986 and 1.25 eV which we assign to a pair of transitions from a lower spin-orbit split valence band [11] to the lowest empty conduction band (labeled $E_{2\pm}$). At still higher energies, we observe absorption from a second pair of transitions for the third band gap at 1.604 and 1.8 eV due to transitions (labeled $E_{3\pm}$) from the lowest occupied valence band to a higher spin-orbit split conductance band. The observed optical transitions at the Γ point are shown schematically in Fig. 4(d). The transition energies (solid lines) are compared with the transition energies predicted by several local density approximation (LDA)/GW band structure calculations [14,15,23,24] (symbols) shown in Fig. 4(e). The absolute values of the band gaps are in generally good agreement with theory, and the spin-orbit splittings of the lower valence band (0.264 eV) and upper conduction band (0.196 eV) are also in good agreement with the predicted values. These higher band gaps are also consistent with those

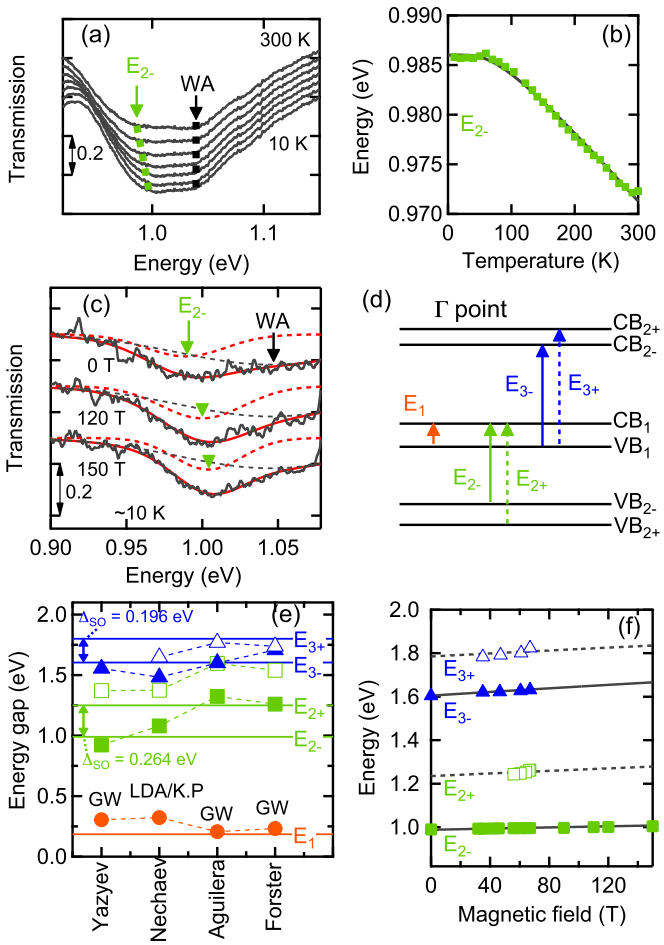

FIG. 4. (a) Transmission spectra of Bi_2Se_3 around 1.0 eV at 0 T at temperatures of 10 and 50–300 K (50 K step). (b) Temperature dependence of second band-gap energy. The solid line shows fitting as described in the text. (c) Low-temperature magnetotransmission spectra at different magnetic fields. Spectra in (a) and (c) are shifted vertically for clarity and the weak feature labeled WA is due to water vapor absorption. (d) Schematic picture of the band structure in bulk Bi_2Se_3 at the Γ point. (e) Energy gap values compared to theoretical predictions from Refs. [14,15,23,24]. (g) Magnetic field dependence of the second and third band gaps with their split-off bands.

(1.0 and 1.6 eV) estimated from fitting the dielectric functions of bulk Bi_2Se_3 at 300 K as reported in Ref. [17], although the spin-orbit splitting could not be resolved. It is also possible that due to the n-type doping, some contribution to the E_{3+} transition could come from a CB_1 to CB_{2+} transition which should occur at the same energy, in a similar process to the two-photon photoemission measurements of the second surface state [25], which may explain why this transition is particularly strong [Fig. 1(a)].

We now examine the temperature and magnetic field dependence of the higher-energy absorptions. Figure 4(a) shows the temperature dependence of the transmission spectra at temperatures of 10 and 50–300 K (50 K step). The E_{2-} transition around 0.99 eV from the lower spin-orbit split valence band (second band gap) shows a clear shift towards higher energies with decreasing temperature, which is plotted in Fig. 4(b) (the small feature labeled WA is a water absorption

around 1.04 eV [26].) The temperature dependence was fitted using the well-known expression for the temperature dependence of a semiconductor band gap [27],

$$E_g(T) = E_g(0) - S\langle\hbar\omega\rangle\left[\coth\left(\frac{\langle\hbar\omega\rangle}{2k_BT}\right) - 1\right], \qquad (2)$$

where $E_g(T)$ is the band gap at the temperature T with $E_g(0) = 0.986$ eV, $S = 0.423$ is a dimensionless coupling constant, and $\langle\hbar\omega\rangle = 19.4$ meV is the average phonon energy. The average phonon energy is within the range of optical phonon energies (4.6–21.6 meV) seen in the Raman spectroscopy in the literature [28].

Figure 4(c) shows the magnetic field dependence of the transmission spectra $T(B)$ at 0, 120, and 150 T, measured using a supercontinuum light source (white-light laser) in the range 1.1–1.7 μm. A single 20 ns light pulse is synchronized with the magnetic field pulse from the single-turn coil and the spectrometer acquisition window. The light pulse is beamsplit and the sample transmission normalized against the same pulse to account for pulse-to-pulse variability. The E_{2-} around 0.99 eV at 0 T shows a small but clear shift towards higher energy with increasing magnetic fields (~15 meV shift at 150 T) and a field-induced increase in intensity. This small diamagnetic shift compared to the essentially linear shift of ~100 meV (Fig. 2) seen for the fundamental band gap is consistent with the assignment of this transition as a strongly bound excitonic state associated with the second band gap, compared to the free-carrier behavior of the E_1 transitions. The increase in intensity and shift produced by the magnetic field also result in the strong differential transmission signals seen in Fig. 1 for the $E_{2\pm}$ and $E_{3\pm}$ transitions, which allows them to be distinguished from the higher quantum number interband Landau-level transitions of band gap E_1 seen in a similar energy range in Fig. 1(a).

The relative strengths of the band edge E_{2-} transition and the higher Landau-level E_1 transitions can be seen in Fig. 1(b) from the magnetic-field-dependent transmission in the 100 T range of magnetic fields at 1.0 eV where changes as large as 20% can be seen, compared to the few percent changes for the higher Landau levels. This is further evidence that the E_{2-} and E_{3-} transitions are not high-order Landau levels of the fundamental band gap, but the lowest interband Landau-level transitions of the second and third band gaps with intensities enhanced by excitonic interactions. Such behavior is typical of that seen, for example, in magnetotransmission studies in the 100 T range of magnetic fields for excitonic states in GaSe [29] and the organic lead-halide perovskite $CH_3NH_3PbI_3$ [30].

The exciton diamagnetic shift can be used to estimate some properties of the higher band-gap excitonic states using the expression [31,32]

$$\Delta E_g(B) = \frac{e^2\langle r^2\rangle B^2}{8\mu}, \qquad (3)$$

which does not require a knowledge of the dielectric constant and where r is the size of the exciton wave function and μ is the exciton-reduced effective mass between the CB_1 and VB_{2-} interband transitions. Recent $\mathbf{k}\cdot\mathbf{p}$ calculations [23] suggest that the effective masses in the lower valence band and upper conduction bands will be comparable to those for CB_1 and VB_1, allowing us to approximate μ to be on the order of $\mu = 0.1m_0$. This means that Eq. (3) predicts that the exciton size is only on the order of $\sqrt{\langle r^2\rangle} = 1.8$ nm. This seems surprisingly small given the well-known high values for the dielectric constant of Bi_2Se_3, which has been shown to be of order 30 even up to photon energies as high as 2 eV [17]. However, such a value would be consistent with the idea that there is a significant excitonic contribution to these higher band transitions which influences the band edge absorption. The difference in absorption behavior and diamagnetic shift between the E_1 and E_{2-} band gaps suggests that there is a significant difference in the physical scale of the excitations from the two different valence bands, which may be related to the difference between the E_1 bulk band gap observed in absorption and that seen in ARPES (0.3 eV), sampled in a different region of the material.

In conclusion, we have used magnetospectroscopy over a wide range of energies (0.55–2.2 eV) and magnetic fields up to 150 T to investigate the bulk band structure of the topological insulator Bi_2Se_3. The interband Landau-level transitions of the fundamental band gap are observed to deviate from the previously reported [16] linearity at high energies, but can be described by a 4×4 massive Dirac Hamiltonian with a negative mass term arising from band inversion caused by strong spin-orbit coupling. Furthermore, in high magnetic fields, the differential absorption spectra $T(B)/T(0)$ reveal strong resonances which were assigned as the lowest interband Landau-level transitions of the second and third band gaps observed at high energies around 0.99 and 1.6 eV, with clearly resolved spin-orbit splittings. From their temperature and magnetic field dependence, they were assigned as excitonic band edge transitions for these higher band gaps.

This work was supported by LNCMI-CNRS, member of the European Magnetic Field Laboratory (EMFL), and by EPSRC (U.K.) via its membership to the EMFL (Grants No. EP/N01085X/1 and No. NS/A000060/1), the TERASPEC project of the Emergence program of IDEX Toulouse, and MEGATER project funded by NEXT Toulouse, by ANR JCJC project milliPICS, the Région Midi-Pyrénées under Contract No. MESR 13053031, the BLAPHENE and STRABOT projects under IDEX program Emergence, and by "Programme Investissements d'Avenir" under the program ANR-11-IDEX-0002-02, Reference No. ANR-10-LABX-0037-NEXT. This work arises from research funded by the John Fell Oxford University Press Research Fund. L.B.D. acknowledges financial support from EPSRC and the Science and Technology Facilities Council (U.K.).

[1] M. Z. Hasan and C. L. Kane, Rev. Mod. Phys. **82**, 3045 (2010).
[2] X.-L. Qi and S.-C. Zhang, Rev. Mod. Phys. **83**, 1057 (2011).
[3] Y. Ando, J. Phys. Soc. Jpn. **82**, 102001 (2013).
[4] A. R. Mellnik, J. S. Lee, A. Richardella, J. L. Grab, P. J. Mintun, M. H. Fischer, A. Vaezi, A. Manchon, E.-A. Kim, N. Samarth, and D. C. Ralph, Nature (London) **511**, 449 (2014).

[5] K. Kondou, R. Yoshimi, A. Tsukazaki, Y. Fukuma, J. Matsuno, K. S. Takahashi, M. Kawasaki, Y. Tokura, and Y. Otani, Nat. Phys. **12**, 1027 (2016).

[6] Y. Xia, D. Qian, D. Hsieh, L. Wray, A. Pal, H. Lin, A. Bansil, D. Grauer, Y. S. Hor, R. J. Cava, and M. Z. Hasan, Nat. Phys. **5**, 398 (2009).

[7] D. Hsieh, Y. Xia, D. Qian, L. Wray, J. H. Dil, F. Meier, J. Osterwalder, L. Patthey, J. G. Checkelsky, N. P. Ong, A. V. Fedorov, H. Lin, A. Bansil, D. Grauer, Y. S. Hor, R. J. Cava, and M. Z. Hasan, Nature (London) **460**, 1101 (2009).

[8] Y. L. Chen, J. G. Analytis, J.-H. Chu, Z. K. Liu, S.-K. Mo, X. L. Qi, H. J. Zhang, D. H. Lu, X. Dai, Z. Fang, S. C. Zhang, I. R. Fisher, Z. Hussain, and Z.-X. Shen, Science **325**, 178 (2009).

[9] D. Hsieh, Y. Xia, D. Qian, L. Wray, F. Meier, J. H. Dil, J. Osterwalder, L. Patthey, A. V. Fedorov, H. Lin, A. Bansil, D. Grauer, Y. S. Hor, R. J. Cava, and M. Z. Hasan, Phys. Rev. Lett. **103**, 146401 (2009).

[10] H. Zhang, C.-X. Liu, X.-L. Qi, X. Dai, Z. Fang, and S.-C. Zhang, Nat. Phys. **5**, 438 (2009).

[11] C.-X. Liu, X.-L. Qi, H. J. Zhang, X. Dai, Z. Fang, and S.-C. Zhang, Phys. Rev. B **82**, 045122 (2010).

[12] K. W. Post, B. C. Chapler, L. He, X. Kou, K. L. Wang, and D. N. Basov, Phys. Rev. B **88**, 075121 (2013).

[13] B. A. Piot, W. Desrat, D. K. Maude, M. Orlita, M. Potemski, G. Martinez, and Y. S. Hor, Phys. Rev. B **93**, 155206 (2016).

[14] O. V. Yazyev, E. Kioupakis, J. E. Moore, and S. G. Louie, Phys. Rev. B **85**, 161101 (2012).

[15] I. Aguilera, C. Friedrich, G. Bihlmayer, and S. Blügel, Phys. Rev. B **88**, 045206 (2013).

[16] M. Orlita, B. A. Piot, G. Martinez, N. K. Sampath Kumar, C. Faugeras, M. Potemski, C. Michel, E. M. Hankiewicz, T. Brauner, Č. Drašar, S. Schreyeck, S. Grauer, K. Brunner, C. Gould, C. Brüne, and L. W. Molenkamp, Phys. Rev. Lett. **114**, 186401 (2015).

[17] M. Eddrief, F. Vidal, and B. Gallas, J. Phys. D **49**, 505304 (2016).

[18] L. J. Collins-McIntyre, S. E. Harrison, P. Schönherr, N.-J. Steinke, C. J. Kinane, T. R. Charlton, D. Alba-Veneroa, A. Pushp, A. J. Kellock, S. S. P. Parkin, J. S. Harris, S. Langridge, G. van der Laan, and T. Hesjedal, Europhys. Lett. **107**, 57009 (2014).

[19] L. Collins-McIntyre, W. Wang, B. Zhou, S. Speller, Y. Chen, and T. Hesjedal, Phys. Status Solidi B **252**, 1334 (2015).

[20] R. J. Nicholas, P. Y. Solane, and O. Portugall, Phys. Rev. Lett. **111**, 096802 (2013).

[21] K. Eto, Z. Ren, A. A. Taskin, K. Segawa, and Y. Ando, Phys. Rev. B **81**, 195309 (2010).

[22] J. G. Analytis, J.-H. Chu, Y. Chen, F. Corredor, R. D. McDonald, Z. X. Shen, and I. R. Fisher, Phys. Rev. B **81**, 205407 (2010).

[23] I. A. Nechaev and E. E. Krasovskii, Phys. Rev. B **94**, 201410 (2016).

[24] T. Förster, P. Krüger, and M. Rohlfing, Phys. Rev. B **92**, 201404 (2015).

[25] J. A. Sobota, S.-L. Yang, A. F. Kemper, J. J. Lee, F. T. Schmitt, W. Li, R. G. Moore, J. G. Analytis, I. R. Fisher, P. S. Kirschmann, T. P. Devereaux, and Z.-X. Shen, Phys. Rev. Lett. **111**, 136802 (2013).

[26] J. R. Collins, Phys. Rev. **26**, 771 (1925).

[27] K. P. O'Donnell and X. Chen, Appl. Phys. Lett. **58**, 2924 (1991).

[28] J. Zhang, Z. Peng, A. Soni, Y. Zhao, Y. Xiong, B. Peng, J. Wang, M. S. Dresselhaus, and Q. Xiong, Nano Lett. **11**, 2407 (2011).

[29] K. Watanabe, K. Uchida, and N. Miura, Phys. Rev. B **68**, 155312 (2003).

[30] A. Miyata, A. Mitioglu, P. Plochocka, O. Portugall, J. T.-W. Wang, S. D. Stranks, H. J. Snaith, and R. J. Nicholas, Nat. Phys. **11**, 582 (2015).

[31] N. Miura, *Physics of Semiconductors in High Magnetic Fields* (Oxford University Press, Oxford, UK, 2008).

[32] S. N. Walck and T. L. Reinecke, Phys. Rev. B **57**, 9088 (1998).